

Migration Behavior of Bead-spring Dumbbell Models under Microchannel Flow from Dissipative Particle Dynamics Simulations

Kwang Jin Oh

Supercomputing Center, Korea Institute of Science and Technology Information, Daejeon 305-806, Korea

E-mail: koh@kisti.re.kr

Received September 17, 2007

Dissipative particle dynamics simulations of bead-spring dumbbell models under microchannel flow were performed and the effects of the deformation on their migration behavior were discussed. Dumbbells were found to migrate toward the walls or the channel center depending on the stiffness. Stiff dumbbells migrated toward the walls. In any cases, the dumbbells were found to have a stronger tendency to move toward the channel center in more deformable conditions.

Key Words : Dissipative particle dynamics simulation, Microchannel flow, Polymer migration

Introduction

Polymer migration under microchannel flow has been paid much attention due to an important implication in polymer engineering such as novel separation and molecular weight fractionation techniques.¹⁻¹¹ For example, polymers in solution migrate away from solid walls. This migration with respect to the flowing solvent particles leads to the formation of a depletion layer near the walls. Since the depletion layer results in higher flow rates near the walls, it would affect rheological properties of the polymer solution. This is practically important for designing microfluidic devices¹² such as lab-on-a chip and microneedle.

Theoretically, continuum mechanics¹³ could be first candidate to study polymers under microchannel flow. However, the validity of the continuum mechanic generally does not hold for polymer solution under microchannel flow. The size of a typical microchannel is an order of micrometer and comparable to the length of polymer, for instance, DNA. Note that the uncoiled length of a λ -DNA is about $22 \mu\text{m}$ ¹⁴ to $32.8 \mu\text{m}$.¹⁵ Therefore, Knudsen number is close to 1. As is well known, when the Knudsen number is much less than 1, the polymer solution can be treated as continuum and continuum mechanics can be employed. However, when the Knudsen number is close to 1, the polymer solution may not be handled by the continuum mechanics. This is largely because polymer deformation may have significant effects on the microchannel flow.

Computer simulation such as molecular dynamics (MD) simulation,¹⁶ Brownian dynamics (BD) simulation,¹⁶ dissipative particle dynamics (DPD) simulation,¹⁷⁻²⁰ and lattice-Boltzmann (LB) simulation²¹⁻²³ can handle the effects, at least, in a coarse-grained level. In this sense, computer simulation is a good candidate as an alternative to the continuum mechanics. Molecular dynamics simulation is most accurate and promising, but computationally intensive for the mesoscopic scale problems and challenging even with the current state-of-art parallel computers. Due to high computational cost of MD simulation, relatively cheap

mesoscale techniques such as DPD simulation, BD simulation, and LB simulation have been widely used for the mesoscale problems.

Unlike BD simulation and LB simulation, the gas-like nature of Schmidt number from DPD simulation has been criticized for polymer simulation²⁴⁻³⁴ under flow since hydrodynamic interactions could be still developing on the time scale of polymer motion.¹⁹ Lowe proposed that the thermostat itself has a viscosity and this fact offers a solution to the problem.²⁰ If the missing viscosity can be replaced by the thermostat contribution to the viscosity, then liquid-like dynamics can be recovered. In addition to the methodological attempt, recent DPD studies, even using the conventional scheme, suggested that the concerns are not well established and DPD simulation is effective in simulating polymer flow in a variety of situations including in nanochannels.^{11,34}

The purpose of this study is to perform DPD simulations using simple bead-spring dumbbell models and investigate the effects of the dumbbell deformation on their migration behavior under the microchannel flow.

Dissipative Particle Dynamics Simulation

The equations of motion for DPD particles are given by

$$\frac{d\vec{r}_i}{dt} = \vec{v}_i \quad (1)$$

$$\frac{d\vec{v}_i}{dt} = \frac{\vec{f}_i}{m_i} \quad (2)$$

where

$$\vec{f}_i = \sum_{j \neq i} \vec{F}_{ij}^C + \vec{F}_{ij}^D + \vec{F}_{ij}^R. \quad (3)$$

The dissipative or drag force is related to the velocity difference between the particles and acts as a resistance against motion. It is given by

$$\dot{\vec{F}}_{ij}^D = -\gamma\omega^D(r_{ij})(\widehat{r}_{ij} \bullet \dot{\vec{v}}_{ij})\widehat{r}_{ij}, \quad (4)$$

where $r_{ij} = |\dot{\vec{r}}_i - \dot{\vec{r}}_j|$, $\widehat{r}_{ij} = (\dot{\vec{r}}_i - \dot{\vec{r}}_j)/r_{ij}$, $\dot{\vec{v}}_{ij} = \dot{\vec{v}}_i - \dot{\vec{v}}_j$, and γ is a friction or drag factor. The random force introduces a Brownian-like, chaotic character of particles and is given by

$$\dot{\vec{F}}_{ij}^R = \sigma\zeta_{ij}\omega^R(r_{ij})\widehat{r}_{ij}, \quad (5)$$

where σ defines the fluctuation amplitude and ζ_{ij} is a random number drawn from a uniform distribution with zero mean and Δt^{-1} variance where Δt is the integration time step. From the fluctuation-dissipation theorem, $\sigma = 2k_B T \gamma$ and $\omega^D(r_{ij}) = [\omega^R(r_{ij})]^2$. The conservative force is a soft repulsive force representing the effective potential between the groups of fluid molecules assembled in the different DPD particles. The expression is given by

$$\dot{\vec{F}}_{ij}^C = a_{ij}\omega^C(r_{ij})\widehat{r}_{ij} \quad (6)$$

where a_{ij} is the maximum repulsion between a pair of particles.

Finally, the weighting function is given by

$$\omega^R(r_{ij}) = \omega^C(r_{ij}) = 1 - \frac{r_{ij}}{r_c} \quad (7)$$

for $r_{ij} < r_c$. Otherwise, it is zero. In this study, r_c was set to 1.

For DPD particles, we set $a_{ij} = 18.75$ if i and j are fluid particles or beads in polymer. For wall particles, we set $a_{wall} = 5.0$ and use a mixing rule $a_{ij} = \sqrt{a_{ij}a_{wall}}$ to give $a_{ij} = 9.68$ when calculating the interaction between fluid and wall particles.

We used two bead-spring dumbbell models. One is finitely extendable nonlinear elastic (FENE)^{35,36} dumbbell model and the other is Hookean dumbbell model. FENE model has been found to capture most of the important nonlinear rheological properties of polymer and has been commonly used in rheology. In FENE model, the potential energy between bead i and bead j is given by

$$V(r_{ij}) = -\frac{1}{2}kR_0^2 \ln\left[1 - \left(\frac{r_{ij}}{R_0}\right)^2\right] \quad (8)$$

if $r_{ij} < R_0$ where k is spring constant and R_0 is finite extended length. Otherwise, it is infinity. Here R_0 was set to 3.0. In Hookean model, the potential energy is given by

$$V(r_{ij}) = \frac{1}{2}kr_{ij}^2 \quad (9)$$

If Hookean and FENE dumbbells have the same spring constant, there should be little or no difference in the behavior of two models at small elongations.

In addition to the conservative forces, we also applied constant external field in x-direction $\vec{f}^{ext} = g\hat{x}$ to generate Poiseuille flow.

We used Lowe's scheme²⁰ to integrate DPD equations of motion. The integration procedure is as follows. Newton's equations of motion are first integrated over a time step Δt using velocity Verlet algorithm.³⁷ For each particle, with a

probability $\Gamma\Delta t$, where Γ is a bath collision frequency, the velocity is exchanged for a new velocity drawn from a Maxwell-Boltzmann distribution. According to a thorough comparison of integration schemes specifically designed for DPD simulations, Lowe's method was found to be a promising candidate.³⁸ The no-slip boundary condition was applied using the frozen wall particle method by Fan *et al.*⁴

Our system is composed of total 55440 particles (45000 fluid particles, 2700 dumbbells, and 5040 wall particles) in the simulation box with dimension $60 \times 7 \times 30.5$. Initially positions of all particles are drawn from the lattice sites of the face-centered-cubic lattice of density 4. Three layers of the lattice plane are used for wall particles, which are frozen in all simulations presented here. Therefore, 5040 wall particles are located in three layers parallel to the (x, y) plane in each side. Here we located two inner layers at $z = 15.25$. Periodic boundary conditions are applied along x and y directions. In this study, Δt was set to 0.02. We ran total for $t = 12000$ - 16000 and averaged sampling data from $t = 2000$ - 4000 . All simulations were performed using a general purpose molecular dynamics simulation program.³⁹

All units will be given in reduced units otherwise specified. The mass of particle, m , cutoff distance, r_c , and $k_B T$ are set to unity

Results and Discussion

Figure 1 shows fully developed velocity profile from Hookean dumbbell model with $k = 6$ at $\Gamma = 20$. To quantify the velocity profile, it was fitted with the function obtained by assuming power-law fluid,

$$v_x(z) = v_{\max} \left[1 - \left(\frac{|z|}{h} \right)^{\frac{1}{n} + 1} \right], \quad (10)$$

where h ($=15.25$) is the channel half-width. When $n = 1$, the power-law fluid equation describes Newtonian fluid. When $n < 1$, it describes a generalized Newtonian fluid with shear-thinning. On the other hand, when $n > 1$, it describes a

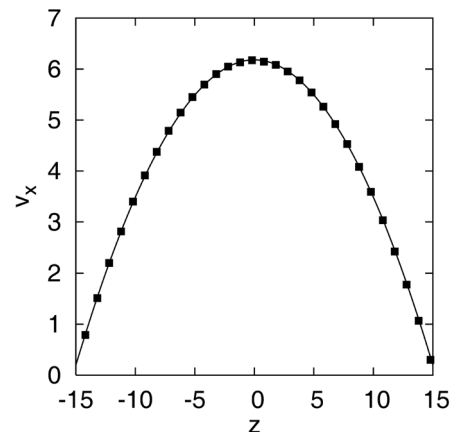


Figure 1. Fully developed velocity profile from Hookean dumbbell model with $k = 6$ and $\Gamma = 20$. The fitted power-law function is also shown.

Table 1. Simulation and model parameter, the fitted values of n and v_{\max} in the power-law fluid equation, the ratio of the radius of gyration to the channel half-width h , the ratio of the volume fraction to the overlap volume fraction, and the Peclet number from each simulation

Model	g	Γ	K	n	v_{\max}	ϕ/ϕ^* ^a	h/R_g	Pe^b
FENE	0.2	20	3	1.005	6.078	0.138	32.585	12.551
FENE	0.2	20	6	1.024	6.138	0.0708	40.667	11.384
FENE	0.02	20	6	1.023	0.611	0.0708	40.667	1.133
FENE	0.6	20	6	0.989	18.919	0.0708	40.667	35.682
FENE	0.2	20	9	1.032	6.167	0.0437	47.806	6.228
Hookean	0.2	20	6	1.034	6.183	0.0337	52.048	5.304
FENE	0.2	2	3	0.581	18.128	0.153	31.447	5.735

^aThe overlap volume fraction ϕ^* is given by $\phi^* = N/4\pi R_g^3 \rho/3$ where N is the number of beads, ρ is density, and R_g is the radius of gyration. ^b $Pe = \dot{\gamma}_w R_g^2$ where the wall shear rate $\dot{\gamma}_w$ is given by $\dot{\gamma}_w = (n + 1/mh) v_{\max}$. The radius of gyration and the diffusion constant D were obtained from free-solution simulation.

generalized Newtonian fluid with shear-thickening. In the figure, we included the fitted function to illustrate that we obtained very good fit overall. For other model systems in this study, which are not shown in the figure, we also obtained very good fit. The fitted values of n and v_{\max} are shown in Table 1. From the table, we can see that the velocity profile is insensitive to the stiffness (*i.e.*, spring constant in the present case). Both n and v_{\max} increases as the stiffness increases. However, the increase is small. On the

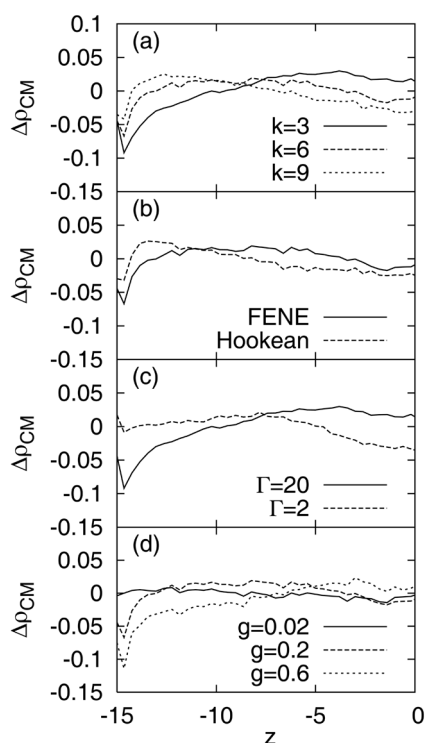


Figure 2. Center-of-mass density profiles from (a) FENE dumbbell models with $k = 3, 6,$ and 9 at $\Gamma = 20$, (b) FENE and Hookean dumbbell models with $k = 6$ at $\Gamma = 20$, (c) FENE models with $k = 3$ at $\Gamma = 2$ and 20 , (d) FENE models with $k = 6$ at $\Gamma = 20$ under $g = 0.02, 0.2,$ and 0.6 . Here the corresponding density profile at $g = 0.0$ was subtracted from each density profile.

other hand, the effect of the bath collision frequency on the velocity profile is quite large. First, n is much less than 1, which indicates that the fluid shows shear-thinning behavior. Second, v_{\max} is about three times larger. The fluid at lower bath collision frequency is less resistant to the flow.

Figure 2 shows the center-of-mass density profile from each model. Here the density profile at $g = 0.0$ was subtracted from each density profile. Therefore positive values at a certain region in the density profile indicate that dumbbells migrated to the region in the presence of a flow. As can be seen from Figure 2, the FENE dumbbells with $k = 9$ are more populated near the walls. On the other hand, the dumbbells with $k = 3$ are more populated at the center region. At $k = 6$, we observe an intermediate distribution, that is to say, two off-center peaks located between the center and the walls. Thus dumbbells show different migration behavior depending on the stiffness. Hookean dumbbell model with the same spring constant as FENE dumbbell model shows the populated region that is shifted toward the walls. The density profile of Hookean dumbbells with $k = 6$ was rather similar to the one of FENE dumbbell with $k = 9$. The bath collision frequency leads to the populated region shifted toward the channel center. Similar behavior was obtained by using higher field strength.

For wide channel ($2h/R_g > 5$), LB simulation data showed that polymer chains migrated toward the channel center in a pressure driven flow. In sufficiently narrow channels, there was a reversal of direction and the polymers moved toward the wall.⁹ Similar behavior was also observed in DPD simulation.¹¹ For relatively long chains, as compared to the channel width, a migration toward the walls was observed. However, for relatively short chains, a migration away from the walls was observed. The present system has very large ratio of the channel width to the polymer size as shown in Table 1. The ratio of the volume fraction to the overlap volume fraction ϕ/ϕ^* is also small (see Table 1). Therefore the confining effects are small. Even for this case, we observed the migration of dumbbells toward either the channel center or the walls depending on the stiffness. This observation is different from the previous results. However the populated region was shifted toward the channel center as the stiffness decreases (Peclet number increases).

In this study, two bath collision frequencies were examined. One is $\Gamma = 2$ and the other is $\Gamma = 20$. Since Schmidt number from DPD simulation using Lowe's scheme is approximately given²⁰ by the formula $S_c = v/D \sim \Gamma^2/k_B T$, which is verified to be true for values satisfying $0 \leq \Gamma \Delta t \leq 0.5$,³¹ $\Gamma = 2$ and 20 correspond to $S_c \sim 4$ and 400 , respectively. At higher bath collision frequency, the populated region was shifted toward the channel center as shown in Figure 2(c). However, Figure 2(a) suggests different migration behavior even at similar Schmidt numbers. This indicates that Schmidt number alone may not be sufficient to describe the migration behavior. The migration behavior was rather more correlated with Peclet number.

Figure 3 shows the stretch profiles under the channel flow. Here the stretch X is defined as $X = X_{\max} - X_{\min}$ where X_{\max}

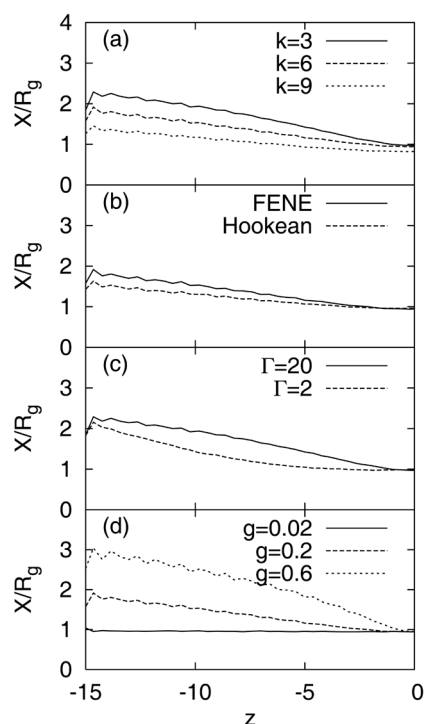


Figure 3. Stretch profiles from (a) FENE dumbbell models with $k = 3, 6,$ and 9 at $\Gamma = 20$, (b) FENE and Hookean dumbbell models with $k = 6$ at $\Gamma = 20$, (c) FENE models with $k = 3$ at $\Gamma = 2$ and 20 , (d) FENE models with $k = 6$ at $\Gamma = 20$ under $g = 0.02, 0.2,$ and 0.6 .

and X_{\min} are maximum and minimum coordinate in x -direction (flow direction) among coordinates of all particles in a polymer, respectively. To compare the stretch with the dumbbell size, we divided the stretch by the radius of gyration in free solution. Under the flow, the strain rate is higher near the walls and zero in the channel center. Therefore the stretch is larger near the walls while it is close to the radius of gyration in the channel center, as can be seen in Figure 3. Similar trends are also observed in the angle between the end-to-end vector and the flow direction (see Figure 4). Note that 1 and 0.5 indicate perfect alignment along the flow direction and free rotation, respectively. The dumbbells rotate freely in the channel center (zero strain rate region). As the dumbbells approach the walls (highest strain rate region), the dumbbells align along the flow direction. In all cases, less stiff dumbbells were subject to more deformation and stronger alignment along the flow direction. Here a dumbbell is less stiff when force constant is smaller, the non-linearity is included in the model, or higher bath collision frequency is used.

Thus, the present results suggest that dumbbells has stronger tendency to migrate toward the channel center in more deformable conditions. This may imply that rigid polymer would migrate toward the walls. Previous theoretical studies^{2,3} using rigid polymer model also proposed that a rigid rod polymer shows a net migration away from the channel center and toward the walls. However those studies considered only the mobility gradient due to the rotational anisotropy. Hydrodynamic interactions and steric effects

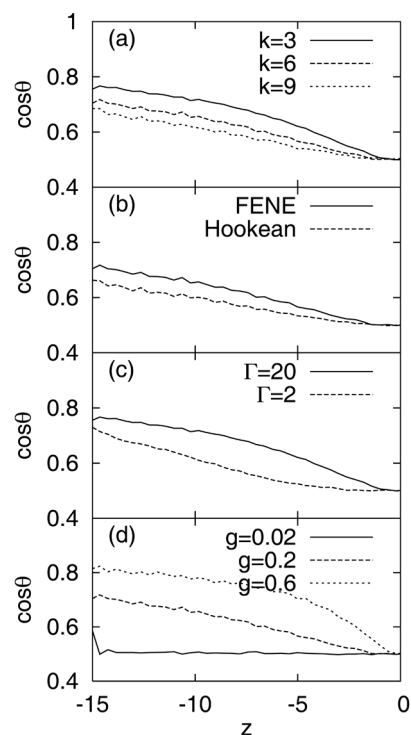


Figure 4. Cosine profiles of the angle between the end-to-end vector and the flow direction from (a) FENE dumbbell models with $k = 3, 6,$ and 9 at $\Gamma = 20$, (b) FENE and Hookean dumbbell models with $k = 6$ at $\Gamma = 20$, (c) FENE models with $k = 3$ at $\Gamma = 2$ and 20 (d) FENE models with $k = 6$ at $\Gamma = 20$ under $g = 0.02, 0.2,$ and 0.6 .

were not considered.

There is the mechanistic view that polymers should tend to migrate toward regions of the flow where their conformational state is least restricted. According to the view, we should observe only migration toward the channel center. Therefore our observations are not explained simply by the mechanistic view and confirm other previous studies.^{6,9,11}

Conclusion

We presented DPD simulation results using bead-spring dumbbell models under microchannel flow. One is FENE dumbbell model and the other is Hookean dumbbell model. In particular, we focused on investigating the effects of dumbbell deformation on their migration behavior. Here we changed the stiffness condition by changing simulation (bath collision frequency) or model parameters (spring constant, non-linearity).

In this study, the ratio of the channel width to the polymer size was large and the ratio of the volume fraction to the overlap volume fraction was small. Consequently the confining effects are small. We found that the dumbbells migrated toward either the channel center or the walls depending on the stiffness. More stiff dumbbells tended to migrate toward the walls. In any cases, when the dumbbells are subject to more deformable conditions, which result in higher Peclet number, the populated region tends to shift toward the channel center.

References

1. Agarwal, U. S.; Dutta, A.; Mashelkar, R. A. *Chem. Eng. Sci.* **1994**, *49*, 1693.
 2. Nitsche, L. C.; Hinch, E. J. *J. Fluid Mech.* **1997**, *332*, 1.
 3. Schiek, R. L.; Shaqfeh, E. S. G. *J. Fluid Mech.* **1997**, *332*, 23.
 4. Fan, X.; Phan-Thien, N.; Yong, N. T.; Wu, X.; Xu, D. *Phys. Fluids* **2003**, *15*, 11.
 5. Jendrejack, R. M.; Schwartz, D. C.; de Pablo, J. J.; Graham, M. D. *J. Chem. Phys.* **2004**, *120*, 2513.
 6. Ma, H.; Graham, M. D. *Phys. Fluids* **2005**, *17*, 83103.
 7. Usta, O. B.; Ladd, A. J. C.; Butler, J. E. *J. Chem. Phys.* **2005**, *122*, 94902.
 8. Khare, R.; Graham, M. D.; de Pablo, J. J. *Phys. Rev. Lett.* **2006**, *96*, 224505.
 9. Usta, O. B.; Butler, J. E.; Ladd, A. J. C. *Phys. Fluids* **2006**, *18*, 31703.
 10. Hernandez-Otiz, J. P.; Ma, H.; de Pablo, J. J.; Graham, M. D. *Phys. Fluids* **2006**, *18*, 123101.
 11. Millan, J. A.; Jiang, W.; Laradji, M.; Wang, Y. *J. Chem. Phys.* **2007**, *126*, 124905.
 12. Koch, M.; Evans, A.; Brunnschweiler, A. *Microfluidic Technology and Applications*; Research Studies Press Ltd.: Hertfordshire, 2000.
 13. Ferziger, J. H.; Peric, M. *Computational Methods for Fluid Dynamics*; Springer-Verlag: Heidelberg, 2002.
 14. Smith, D. E.; Babcock, H. P.; Chu, S. *Science* **1999**, *283*, 1724.
 15. Bustamante, C.; Marko, J. F.; Siggia, E. D.; Smith, S. *Science* **1994**, *265*, 1500.
 16. Allen, M. P.; Tildesley, D. J. *Computer Simulation of Liquids*; Oxford: Clarendon, 1987.
 17. Hoogerbrugge, P. J.; Koelman, J. M. V. A. *Europhys. Lett.* **1992**, *19*, 155.
 18. Koelman, J. M. V. A.; Hoogerbrugge, P. J. *Europhys. Lett.* **1993**, *21*, 369.
 19. Groot, R. D.; Warren, P. B. *J. Chem. Phys.* **1997**, *107*, 4423.
 20. Lowe, C. P. *Europhys. Lett.* **1999**, *47*, 145.
 21. Ladd, A. J. C. *J. Fluid Mech.* **1994**, *271*, 285.
 22. Alhrichs, P.; Dunweg, B. *J. Chem. Phys.* **1999**, *111*, 8225.
 23. Ladd, J. C.; Verberg, R. *J. Stat. Phys.* **2001**, *104*, 1191.
 24. Kong, Y.; Manke, C. W.; Madden, W. G.; Schlijper, A. G. *Int. J. Thermophys.* **1994**, *15*, 1093.
 25. Schlijper, A. G.; Hoogerbrugge, P. J.; Manke, C. W. *J. Rheol.* **1995**, *39*, 567.
 26. Schlijper, A. G.; Hoogerbrugge, P. J.; Manke, C. W. *J. Rheol.* **1995**, *39*, 567.
 27. Kong, Y.; Manke, C. W.; Madden, W. G.; Schlijper, A. G. *J. Chem. Phys.* **1997**, *107*, 1.
 28. Spenley, N. A. *Europhys. Lett.* **2000**, *49*, 534.
 29. Lowe, C. P.; Bakker, A. F.; Dreischor, M. W. *Europhys. Lett.* **2004**, *67*, 397.
 30. Symeonidis, V.; Karniadakis, G. E.; Caswell, B. *Phys. Rev. Lett.* **2005**, *95*, 76001.
 31. Symeonidis, V.; Karniadakis, G. E.; Caswell, B. *Bull. Pol. Acad. Sci. Tech. Sci.* **2005**, *53*, 395.
 32. Chen, L.-J.; Lu, Z.-Y.; Qian, H.-J.; Li, Z.-S.; Sun, C.-C. *J. Chem. Phys.* **2005**, *122*, 104907.
 33. Symeonidis, V.; Karniadakis, G. E.; Caswell, B. *J. Chem. Phys.* **2006**, *125*, 184902.
 34. Jiang, W.; Huang, J.; Wang, Y.; Laradji, M. *J. Chem. Phys.* **2007**, *126*, 44901.
 35. Bird, R. B.; Curtiss, C. F.; Armstrong, R. C.; Hassanger, O. *Dynamics of Polymeric Liquids, Kinetic Theory*; Wiley: New York, 1987; Vol. 2.
 36. Kröger, M. *Phys. Rep.* **2004**, *390*, 453.
 37. Andersen, H. C. *J. Chem. Phys.* **1980**, *72*, 2384.
 38. Nikunen, P.; Karttunen, M.; Vatturainen, I. *Comp. Phys. Comm.* **2003**, *153*, 407.
 39. Oh, K. J.; Klen, M. L. *Comp. Phys. Comm.* **2006**, *174*, 560.
-